

Naval Research Laboratory

Washington, DC 20375-5320



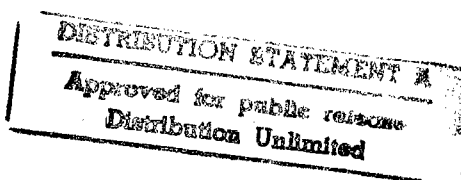
NRL/MR/6176-92-7135

Ion-Beam-Assisted Deposition of MoS₂ and Other Low-Friction Films

ROBERT N. BOLSTER

*Surface Chemistry Branch
Chemistry Division*

September 11, 1992



19980309 110

PLEASE RETURN TO:
BMD TECHNICAL INFORMATION CENTER
BALLISTIC MISSILE DEFENSE ORGANIZATION
7100 DEFENSE PENTAGON
WASHINGTON D.C. 20301-7100
DTIC QUALITY INSPECTED 4

Approved for public release; distribution is unlimited.

U5689

Accession Number: 5689

Publication Date: Sep 11, 1992

Title: Ion-Beam-Assisted Deposition of MoS₂ and Other Low-Friction Films

Personal Author: Bolster, Robert N.

Corporate Author or Publisher: Naval Research Laboratory, Surface Chemistry Branch, Washington, DC 20375-5320

Report Number: NRL MR 6176-92-7135

Report Prepared For: Air Force Wright Aeronautical Lab (WRDC/MLBT), Wright-Patterson AFB, OH 45433

Descriptors, Keywords: ion beam film deposition MoS₂ solid lubricant sputter friction

Pages: 0034

Cataloged Date: May 25, 1995

Document Type: HC

Number of Copies in Library: 000001

Record ID: 46340

REPORT DOCUMENTATION PAGE			Form Approved OMB No. 0704-0188	
Public reporting burden for this collection of information is estimated to average 1 hour per response, including the time for reviewing instructions, searching existing data sources, gathering and maintaining the data needed, and completing and reviewing the collection of information. Send comments regarding this burden estimate or any other aspect of this collection of information, including suggestions for reducing this burden, to Washington Headquarters Services, Directorate for Information Operations and Reports, 1215 Jefferson Davis Highway, Suite 1204, Arlington, VA 22202-4302, and to the Office of Management and Budget, Paperwork Reduction Project (0704-0188), Washington, DC 20503.				
1. AGENCY USE ONLY (Leave Blank)		2. REPORT DATE September 11, 1992		3. REPORT TYPE AND DATES COVERED Interim 6/88 to 6/92
4. TITLE AND SUBTITLE Ion-Beam-Assisted Deposition of MoS ₂ and Other Low-Friction Films			5. FUNDING NUMBERS PE - 63224C, 61153N WU - 2855, 3409	
6. AUTHOR(S) Robert N. Bolster				
7. PERFORMING ORGANIZATION NAME(S) AND ADDRESS(ES) Naval Research Laboratory Washington, DC 20375-5320			8. PERFORMING ORGANIZATION REPORT NUMBER NRL/MR-6176-92-7135	
9. SPONSORING/MONITORING AGENCY NAME(S) AND ADDRESS(ES) Department of the Air Force Air Force Wright Aeronautical Lab. (WRDC/MLBT) Wright-Patterson Air Force Base, OH 45433			10. SPONSORING/MONITORING AGENCY REPORT NUMBER	
11. SUPPLEMENTARY NOTES				
12a. DISTRIBUTION/AVAILABILITY STATEMENT Approved for public release; distribution is unlimited.			12b. DISTRIBUTION CODE	
13. ABSTRACT (Maximum 200 words) Vacuum-deposited films of molybdenum disulfide (MoS ₂) are effective as solid lubricants. Ion-beam-assisted deposition, which employs ion beam sputtering with an assist beam impinging on the growing film, has been investigated as a means of preparing low-friction high endurance coatings. The apparatus used and some of the techniques involved are described. Ion source operating parameters were optimized and the assist beam ion flux was quantified and found to follow a power-law relationship with beam power. The best way to produce MoS ₂ films was found to be cosputtering from separate Mo and S targets with deposition rates adjusted to obtain the desired stoichiometry. Deposition rates were found to also follow a power-law relationship with beam power, and formulae are given for predicting them, the ratio of assist ions to film atoms, and the effect of assist beam sputtering on film thickness. Inverse formulae are given for determining process parameters needed to achieve a selected film thickness and composition. A composite target for simultaneous Mo and S sputtering was developed. Deposition rates were determined for other metals: W, Ni, Co, Cu, and Pb. Formulae relating target-to-substrate distance to deposition rate are given.				
14. SUBJECT TERMS Ion beam Film deposition			15. NUMBER OF PAGES 34	
MoS ₂ Solid lubricant			16. PRICE CODE	
Sputter Friction				
17. SECURITY CLASSIFICATION OF REPORT UNCLASSIFIED		18. SECURITY CLASSIFICATION OF THIS PAGE UNCLASSIFIED		19. SECURITY CLASSIFICATION OF ABSTRACT UNCLASSIFIED
				20. LIMITATION OF ABSTRACT UL

CONTENTS

BACKGROUND	1
APPARATUS	1
Vacuum Chamber	2
Target Holders	2
Targets	3
Ion Sources	4
Stage	5
Quartz Monitor	6
Residual Gas Analyzer	6
Gas Supply	7
PROCEDURES	8
Deposition	8
Thickness Measurement	9
Ion Sources	10
ASSIST BEAM FLUX MEASUREMENT	13
DEPOSITION RATE CONTROL	15
MoS ₂ and Sulfur	15
Molybdenum and Sulfur	15
Improved Mo and S Data	19
Assist Beam Effects	20
Film and Process Parameter Calculation Summary	23
Composite Mo-S Target	25
Deposition of Various Metals	26
Effect of Target Distance	27
Uniformity of Deposition	27
Intentional Composition Gradients	28
SUMMARY	28
ACKNOWLEDGMENTS	29
REFERENCES	29

ION-BEAM-ASSISTED DEPOSITION OF MoS₂ AND OTHER LOW-FRICTION FILMS

BACKGROUND

Films of the solid lubricant molybdenum disulfide (MoS₂) deposited by vacuum processes such as rf or dc sputtering have been found effective for the lubrication of bearings in vacuum environments. The Naval Research Laboratory has established a facility for the laboratory scale preparation of such films by ion beam sputtering. In this process beams of ions, usually of the inert gas argon (Ar), bombard targets imparting sufficient energy that atoms are emitted from the target and deposited as a film on nearby substrates. In addition to controlled deposition of one or more materials, this process allows ion-beam-assisted deposition (IBAD), where an ion beam directed at the substrate modifies the composition and structure of the film as it forms.

Over several years numerous MoS_x films have been prepared and some of their properties have been reported (1,2,3). These include low friction coefficients, typically 0.01 to 0.02, and remarkable endurance under highly-loaded sliding contact (less than an atomic layer per cycle). In this report more of the experimental details and practical procedures than could be included in other publications are collected for use by other researchers or for transition to industry.

APPARATUS

The apparatus consists of a vacuum chamber mounted atop a cabinet containing the high-vacuum pump and various utilities; a console containing the ion source power supplies, controls, and instrumentation; and various accessories such as the mechanical

Manuscript approved July 30, 1992.

vacuum pump and a gas supply system. The basic apparatus was built to our specifications by Commonwealth Scientific Corporation of Alexandria, Virginia. A number of accessories have been added and modifications made to the system to increase its capabilities.

Vacuum Chamber

The vacuum chamber is cylindrical, 51 cm (20 inches) in diameter and 46 cm (18 inches) deep, with its axis horizontal. One end opens to provide access to the interior. The walls are stainless steel, with numerous welded ports for the ion sources, pressure gauges, and other accessories. There are removable liners to facilitate cleaning, and a bake-out jacket. The chamber is rough-pumped by a 760 L/min mechanical pump and automatically crosses over to a cryogenic high-vacuum pump with a pumping speed of 4000 L/s for water and 1200 L/s for argon. The normal base pressure is about 10^{-7} Torr (10^{-5} Pa). When the ion sources are operating the pressure is in the range of 2 to 6×10^{-4} Torr. A high-vacuum manipulator has been installed so that substrates can be moved, covered or uncovered while under vacuum. This permits making several types or thicknesses of films in one run. A diagram of the chamber and its contents is shown in Fig. 1.

Target Holders

Two water-cooled holders for four sputtering targets are provided. The targets are selected remotely from the operating console. Early films showed considerable nickel contamination, apparently the result of sputtering from the nickel-plated holder block and shields by the outer portion of the ion beam. The left target holder has been fitted with a graphite foil shield to prevent the beam from striking any metallic surfaces.

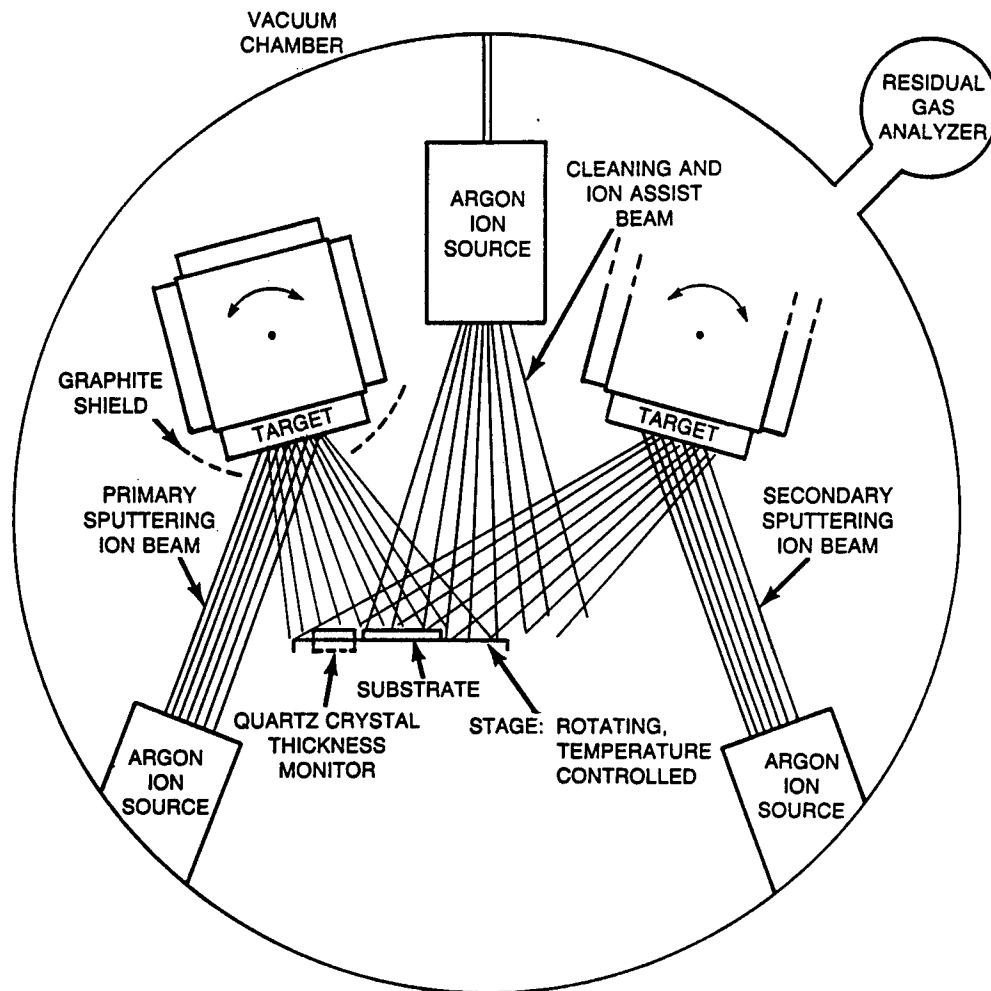


Fig. 1 - Arrangement of the major components in the IBAF apparatus vacuum chamber as seen from the front with the stage in the left position. The quartz crystal monitor shown beside the substrate here for clarity was actually directly behind it.

Targets

Most of the targets are in the form of 3-inch (7.6 cm) disks 1/4 in. (6.4 mm) thick cemented by silver-filled epoxy to copper backing plates, which are mounted on the holder by threaded studs. Silver-filled vacuum grease between the backing plate and the target holder assists the transfer of heat from the target.

A sulfur (S) target has been prepared by allowing a pool of molten sulfur to solidify on a recessed copper disk to which a copper screen had been soldered. The screen provides improved adhesion and thermal conductance. The target is replenished by heating it until the sulfur melts (119°C) and adding additional sulfur. Shrinkage or porosity which occurs during crystallization is patched by local melting with a soldering gun.

Ion Sources

The three ion sources are of the Kaufman type (4,5). Gas, normally Ar, is supplied to a discharge chamber at the rate of a few standard cubic centimeters per minute (SCCM). Electrons from a hot filament cathode are accelerated toward the cylindrical anode which forms the walls of the chamber, ionizing the gas atoms or molecules by impact. The efficiency of this ionization is increased by a magnetic field provided by permanent magnets outside the chamber. The positively charged ions are accelerated away from the anode by the high voltage provided by the beam power supply. Passing through aligned holes in the screen grid and accelerator grid, the ions form beamlets which merge to form the ion beam. Immersed in the beam is a heated tungsten filament which emits electrons to neutralize the positive charge of the beam.

The sources produce beams of 3 cm diameter, with beam energies (voltages) of 50 to 1500 V and maximum currents of 100 mA. The two sources used for sputtering are equipped with graphite grids to produce high-intensity beams, the left source usually with focussed grids and the right with collimated grids giving a slightly larger beam. The assist source has convex molybdenum grids to produce a broader low intensity beam. Operating in manual mode with maximum accelerator (grid) voltage of 500 V also helps to broaden the assist beam.

Stage

The substrate stage consists of a circular platen 11.5 cm in diameter supported by the stage assembly. Threaded holes around the periphery facilitate the use of plates or wire loops to hold substrates in place. The platen is motor driven in rotation to improve the uniformity of deposition, and can be heated to 620 K (350°C). The original temperature sensor was inadequate, indicating a temperature far below actual, and was replaced by a fine-gauge thermocouple inserted into a bronze shoe riding in contact with the edge of the platen.

The stage assembly is mounted to the front plate of the chamber on an eccentric rotating platform with a radius of motion of 3.4 cm which permits limited horizontal and vertical positioning and tilting of the platen. The eccentric platform was normally set 30° to the left of the highest position with the platen horizontal. The stage support also swings in a plane parallel to the platen surface 2.6 cm to either side. Normally swung to the left, the center of the platen was then 4.3 cm left of the chamber center plane, 11.9 cm from the center of the left target and 17.5 cm from the right target. This position minimized the distance to the left target, which normally was the substance with the lower sputter yield.

The chamber was designed with the stage platen facing upward to make possible the coating of loose objects such as bearing balls. This also reduces the fixturing needed for holding flat substrates. A disadvantage of this position is that particles can fall onto the substrates during the process creating defects in the coating.

The platen can be shuttered by a sliding cover operated by a feed-through rod. Three Faraday cups built into the cover serve to check the aim and flux of the assist beam. A larger cup with a

suppressor electrode has been added to provide more accurate beam flux data.

Quartz Monitor

A quartz crystal deposition rate monitor indicates the rate during the process and the total thickness deposited. Mounted on a cylindrical feed-through from the top of the chamber, the crystal can be placed anywhere by raising, lowering and rotating the feed-through or bending the support tubing. For normal operation, repositioning the crystal by manually bending the support is undesirable, so it is placed where different stage positions can be accommodated by rotation of the feed-through alone. With the stage at the left the crystal is located at the same height as the platen and directly behind it (at the same distance from the chamber center plane). The mean "tooling factor" for this position was found to be $160 \pm 20\%$, that is, the film thickness on a substrate at the center of the platen was 1.6 x that on the crystal. With the stage at the center or right positions the crystal is moved as close as possible: near the end of the stage frame but 2 or 3 cm to the left of center, or near the corner of the frame and 5 or 6 cm left of the platen center. Approximate tooling factors for these positions were: center, left target = 120%; center, right target = 180%; right, right target = 260%.

Residual Gas Analyzer

A quadrupole mass spectrometer residual gas analyzer (RGA) with a differential pumping system has been added to the chamber to monitor the composition of the gases present during deposition and to check the purity of the sputtering gas. For qualitative monitoring analog mode (graphic mass spectrum display) was used with subtraction to eliminate the detector background. With the chamber under vacuum and the high-conductance valve open the RGA sampled the residual gases in the chamber at base pressure. During

deposition only a 6-mm bypass valve was open to restrict the flow of gas into the detector. With a three-decade logarithmic analog display showing the major Ar peak at full scale, any gases above 1/1000 the partial pressure of the Ar would be detected. Gas analysis was done in tabular mode, which includes correction factors for ionization efficiency. A computer spreadsheet was used to subtract the background and calculate the composition.

At base pressure the spectrum showed, in addition to the usual atmospheric gases, SO_2 and H_2S dispersed in the chamber as a result of sputtering sulfur and outgassing of the S target. These gases are corrosive and attacked some components of the apparatus, especially copper wires, gaskets, and valve seats. When the chamber was not in use, sheets of clean copper foil were placed in it to take up these gases. During depositions when S was being sputtered a peak about 1/100 the height of the Ar and believed to be due to CS_2 was usually seen. The height of this peak was useful as a rough indicator of the amount of S being produced by sputtering.

Gas Supply

The Ar gas was purified by passing it through powdered copper at 670 K to remove oxygen and through silica gel to remove water. A manifold supplied the gas through flow meters to the ion sources where manual needle valves controlled the flow rates, which were typically 8-10 SCCM for the sputter sources, around 10 SCCM for the assist source when being used for cleaning, and around 3 when it was used to assist during deposition. A connection to the mechanical vacuum pump permitted evacuation of the manifold and supply lines. The manifold also supplied pure nitrogen (N_2) from liquid N_2 boil-off for backfilling the chamber before opening. A reservoir allowed mixtures of Ar and N_2 , or pure N_2 , to be supplied to the assist source to change the composition of the assist ion beam.

Even though the lines from the manifold to the source valves were kept under Ar pressure, when the source gas was first turned on the RGA would show substantial amounts of nitrogen and oxygen for many minutes until the lines were purged. Some of the lines were of polymeric tubing which apparently allows oxygen and nitrogen to diffuse in and contaminate the Ar. Therefore, the lines were evacuated and refilled before each deposition.

PROCEDURES

Deposition

Substrates were placed on the platen, sometimes clamped but more often just restrained by wires to keep them in place. For film thickness measurement a piece of glass microscope slide masked with a piece of razor blade was placed near the substrates. Nickel foil substrates were often used for analysis of the film by Rutherford backscattering spectrometry (RBS). To deposit films of MoS₂ on a base layer (6,2) of titanium nitride (TiN), TiN and Mo targets were mounted in the left target holder and S in the right. The stage was positioned to the left. Before the chamber was closed, pure N₂ gas from a hand-held nozzle was used to blow loose particulates from chamber, ion sources, and substrate surfaces. Three to four hours were allowed for the chamber to pump down to base pressure, typically 3×10^{-7} Torr.

During the coating process the procedure and the operating parameters were recorded on data sheets which are shown in Figs. 2 and 3, filled out with data from a typical run. The processing steps are listed at the bottom of Fig. 2: The substrates were sputter cleaned using the assist beam at 40 mA for 3 minutes with the platen rotating, and in this case heated to 200°C. The TiN target was then selected, and the base layer deposited using the left sputter source at 1100 V and 70 mA, with an assist beam of 3.5 mA. An Ar flow of only 3 to 4 SCCM was needed to operate the

assist source at these low powers. Sputtering was done for one or two minutes to clean the target, then platen rotation was started, the stage cover was withdrawn, and the crystal monitor and timer were started. The ion source operating parameters were recorded in the body of the data sheet. At the top of Fig. 3 periodic rate and thickness data from the crystal monitor were recorded along with the more variable source parameters and other comments or observations.

For the top layer the Mo and S targets were selected and a similar procedure followed. The Mo was usually sputtered at 1000 V and 50 mA, S at 1000 V and about 19 to 20 mA. Assist beam current was set to produce the desired ion/atom ratio, usually 0.03, which required 4 to 5 mA. The quantitative factors involved will be discussed later. In the case shown, an 8.2-mA beam was used, resulting in an ion/atom ratio of 0.075.

Thickness Measurement

The thickness of each film was determined from measurement of the step height at the edge of the masked area on glass with Tolansky interferometry. To make the step uniformly reflective it was coated with sputtered aluminum applied in a separate process with the same apparatus (4 minutes at a beam power of 45 W). This allowed step heights to be measured to an accuracy of 5-10 nm. A correction for the depth of the sputter cleaning etch was added to the step height, and data from the crystal monitor were used to apportion the thickness between the layers. As an example, the data of Fig. 3 show the step height was 280 nm. The correction of 35 nm for the 3-minute cleaning etch was added to give 315 nm, which was 140% of the sum of the crystal monitor thicknesses, acceptably close to the nominal tooling factor of $160 \pm 20\%$. The separate monitor thicknesses were multiplied by 1.4 to give the calculated values.

Coating Data Sheet							
Naval Research Lab., Code 6176							
Substrate		AMS-5749-4, 440C-74				Date 9/1-3-14	
		Masked Glass					
Stage: Mounting		Inclin. 0		Ecc. Angle 30° L		Swing Left	
Temp.: Cool. _____		Heat, set 200°C		Max. 201		Min. 197	
Rotation: Y <input checked="" type="checkbox"/> N _____							
Ion Source:		Left	Left	Right	Assist	Assist	
Pressure: (Each source)		1.9 E-4	1.9 E-4	1.8 E-4	1.7 E-4	8 E-5	Base 2.0 E-7 T
Gas:	Flow, SCCM	9.8	9.9	9.1	8.3	3.4	Alterations or repairs since last run: NONE
Mode: (Auto., Man.)		A	A	A	M	M	
Beam	I, mA	70	50	19.2	40	8.2	
	E, V	1100	1000	1000	1000	1000	
Accelerator	I, mA	2.7	2.6	0.8	1.7	0.5	
	E, V	105	125	122	500	500	
Discharge	I, A	1.77	1.15	0.47	1.58	0.25	
	E, V	40.1	40.1	40.4	41.1	41.0	
Cathode	I, A	4.24	3.46	6.02	8.10	6.55	
Neutralizer	I, A	3.72	3.0	5.41	5.10	6.23	
Neut. Emission, mA		70.1	50	19.5	39.7	8.2	
Beam not neut., mA		≈ 0	0	≈ 0	≈ 0	0	
Target	I, mA	39	16	-			Substrate Covers: Close Open
Process	Target:					I _B , mA	
1.	CLEAN	3 ^m 40 mA	All
2.	BASE	TiN	3.5 mA	"
3.	TOP	Mo	S	8.2 mA	"
4.

Fig. 2 - Coating data sheet, page 1.

Ion Sources

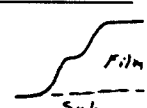
Measurements have shown that sputter deposition rates increased with beam current and energy until, as shown in Fig. 4, a maximum and a sharp drop were found as voltages were increased above 1150 V. It is thought that the beams expand and lose intensity at higher voltages, perhaps due to mutual repulsion of

Coating Data Sheet 2

Date 9/1-3-14

Flow meter zero readings: L= 0.10 R= -0.06 A= 0.12

Base	Time, min.	Å/s	ΣÅ	Left Right		
				I _{Neut.Fil.}	I _{Target}	
TiN	1	0.3-0.4	21	3.90	40	197°C
	3	"	67	3.84	38	P=2.8E-4T
	6	"	134	3.64	39	
	9	"	202	3.51	40	
	10		224			STOPPED
22.4 nm						
Top MoS ₂	1	1.9-2.0	118	3.1	15	197°
	3	2.0-2.2	369	3.06	16	P=4.3E-4T
	6	2.1-2.3	759		17	199°
	9	"	1154	2.7	17	
	12		1534		17	
	15	2.0-2.2	1918	2.5	16	
	16		2043			STOPPED
204 nm						

Thickness: 1.02 fringes = 280 nm 

Plus sub. etch 35 315 nm Total Thickness

Yield = 140 % of Xtal monitor thickness.

	Calc. Thickness	Calc. Rate	R _{calc}
Base	30 nm	3.1 nm/min.	0.09 Ion/Atom
Top	285	17.7	0.075

Fig. 3 - Coating data sheet, page 2.

the ions. Expansion of the beam can be detected visually as the energy approaches 1500 V. Therefore, 1100 V was the maximum, and 1000 V the most commonly used energy. Beams of high intensity are desirable to maximize the sputtering rate and reduce the time needed, but repeatability is even more important in quantifying the relationship between the operating parameters and film composition and properties.

One problem encountered with the sputtering ion sources was that the beams were not always coaxial with the source housings, even though the grids were kept accurately aligned. This caused the beam axes to be off of the target centers, threatening to alter the geometry and sputtering rate or sputter contaminants from the target holders or shields. Beam alignment was difficult to check visually through the viewports, even when operating in manual mode with the neutralizer filaments off. Aluminum foil placed over the targets was useful

in determining the aiming, as the beams would melt a hole in it in a few seconds, marking the position of maximum intensity. Adjustments were made by placing Teflon spacers between the source bodies and their sockets to tilt the axes in the proper directions.

Some care was needed to keep the ion sources operating properly. Neutralizer filaments lasted only about an hour when the source was operated at high power due to erosion of the tungsten wire. New filaments draw about 6 A at high beam currents. The filament current declines steadily as the wire erodes, and failure is imminent when it reaches 3 A. The data in Figs. 2 and 3, for example, show that the left source neutralizer was in need of replacement before the next use.

Cathode filaments last much longer, but replacement may temporarily reduce the maximum attainable beam current to around 25 to 40 mA when the filament power supply reaches its limit. This problem can sometimes be circumvented by placing the new filament

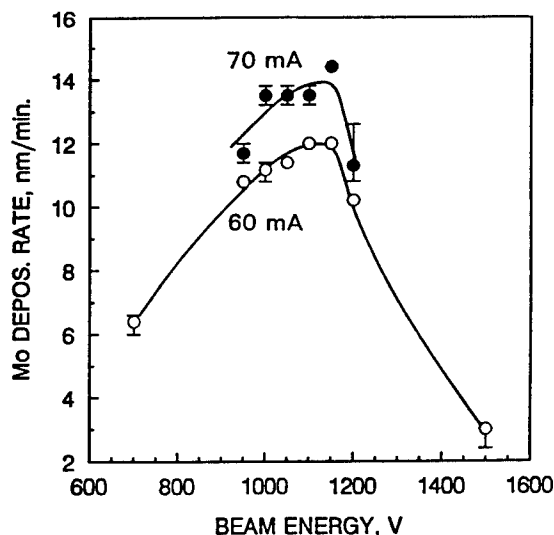


Fig. 4 - Deposition rate for molybdenum sputtered at two beam currents and several beam energies. Bars show the range of the data.

and anode subassembly in the right source and moving the right subassembly with the "broken-in" filament to the left source. Increasing the gas flow rate may also help to increase the beam current. It has been found that a cathode filament can be "broken in" by the following procedure: Turn on the source gas flow. Set power supply to Manual mode, turn on Source power, but leave Beam off. Set Discharge and Cathode at maximum. The cathode current, typically about 8.2 A, will slowly decrease. When it reaches 8.0 A the source should be able to produce a 50 mA beam. Test it and continue the "break-in" process if necessary.

ASSIST BEAM FLUX MEASUREMENT

For many materials, ion beam sputtering deposits more dense films than rf or dc plasma sputtering because it is a higher-energy process. Not only do the sputtered atoms arrive with more energy, but the growing film is also bombarded by energetic reflected ions and atoms. The ion assist beam provides an additional controlled source of energetic ions (7,8). In the deposition of MoS_2 , the assist beam flux affects the orientation and crystallinity and thus the tribological behavior of the film (6,3).

Measurements of the assist ion flux (current density) at various beam currents at 1000 V were made with an electrostatically suppressed Faraday cup having an aperture of 0.25 cm^2 . Placed at the usual substrate-to-source distance of 16 cm, the cup could be traversed across the beam to determine the flux decrease with off-axis distance. A potential of -50 to -140 V, depending upon the ion flux, was applied to the suppressor electrode. The necessary potential was determined by starting with a low value and increasing it until a constant cup current was reached. The chamber pressure was either at a low level, about 1×10^{-4} Torr, or at typical operating level of 4×10^{-4} Torr (0.05 Pa).

Some of the resulting profiles are shown in Fig. 5. The increase in ion flux with current and the effect of pressure can be seen. (Lower pressure increased the flux by reducing the collisions between beam ions and gas.) The ion flux was found to decrease to half of its maximum at a distance of 4 cm from the beam axis. Over a range of beam currents from 1 to 40 mA, the ion flux was found to fit a power law relationship with the beam current so that:

$$F = 3.8 I_B^{1.09} \quad [1]$$

where F is the mean ion flux of the five central measurements (about 5 cm diameter area) in $\mu\text{A}/\text{cm}^2$ and I_B is the beam current in mA. This relationship and the regression line are shown in Fig. 6.

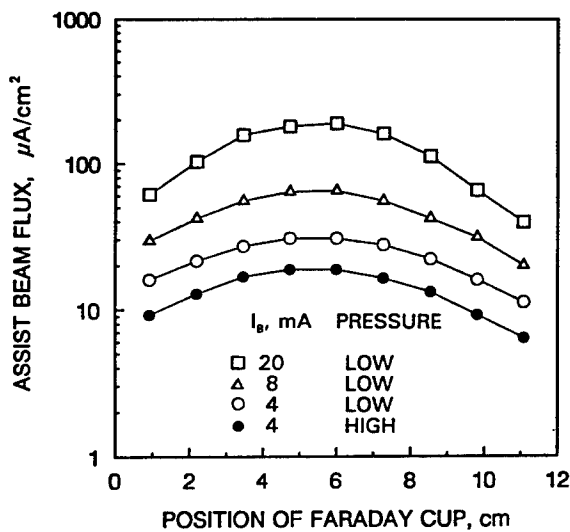


Fig. 5 - Assist beam ion flux profiles at three beam currents and two chamber pressures as a function of distance along the beam diameter. Low pressure $\approx 1 \times 10^{-4}$ Torr, high pressure $\approx 4 \times 10^{-4}$ Torr.

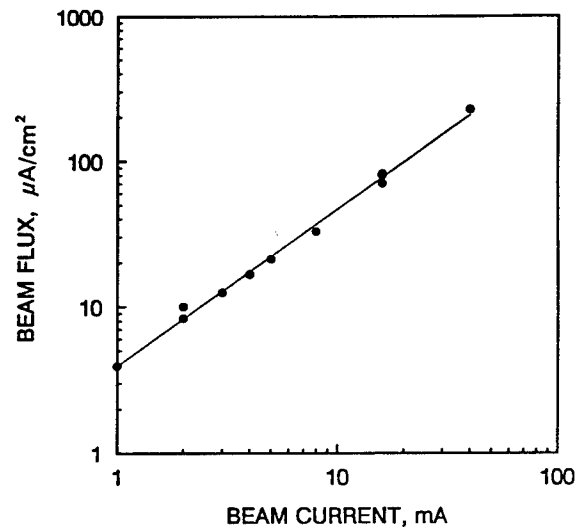


Fig. 6 - Relationship between the mean of the five central measurements of assist beam ion flux and the beam current at a pressure of 4×10^{-4} Torr.

The flux of Eq. [1] does not include bombardment by Ar neutralized by charge exchange collisions in the path between the assist source and the substrate, as they would not be detected by the Faraday cup. The total flux of all energetic particles was probably about $1.5 \times$ larger (9).

DEPOSITION RATE CONTROL

Ordinarily, the highest possible sputter deposition rate is desired in order to expedite the coating process. However, when two different targets are cosputtered to produce a film of mixed composition, the two deposition rates must be known and controlled to give the desired composition.

MoS₂ and Sulfur

Films made by sputtering an MoS₂ target were very depleted of sulfur ($S/Mo = 1.1-1.3$). To achieve stoichiometry by sputtering MoS₂ with a small amount of sulfur added from a S target, it was sufficient to sputter the MoS₂ at the maximum rate and try several S beam powers. The resulting films were analyzed by RBS and the beam power corresponding to a S/Mo ratio of 2 was determined. Stoichiometric films were deposited at rates of 7 to 11 nm/min by this process, using an MoS₂ sputter power of 77 W and a S sputter power around 4 W.

Molybdenum and Sulfur

Cosputtering Mo metal and S to form MoS₂ was found to give higher deposition rates, 15 to 35 nm/min, but with quite varied S/Mo ratios. To achieve the desired stoichiometric ratio more knowledge of the effects of the ion beam parameters on the sputter deposition rates of Mo and S separately was needed.

In order to make immediate deposition rate measurements, the quartz crystal monitor was placed at the usual substrate position, 11.9 cm from the Mo target and 17.5 cm from the S. Deposition rates for Mo were measured at beam energies from 700 to 1500 V and beam currents from 10 to 70 mA. Rates increased with increasing current and energy up to 1150 V. At 1200 V and above the rates declined sharply as noted above in the discussion of Fig. 4. Over the range of 700 to 1100 V, the deposition rate and the beam power closely fit a power law relationship with the log of the deposition rate proportional to the log of the product of beam current and energy, as shown by the rectangular markers in Fig. 7. The equation of the regression line (parallel to but above the line shown) is

$$D_{\text{Mo}} = 0.035 P_{\text{Mo}}^{1.38} \quad [2]$$

where D is the rate in nm/min and P is the sputter beam power in watts.

Similar experiments were then done with the sulfur target yielding much higher rates, shown by the "X" markers in Fig. 7, and a line with a steeper slope (not shown). Subsequent codepositions gave still higher rates. Either the monitor was not accurate in measuring the deposition of pure S, or the sticking coefficient of S is higher when codeposited with Mo than when it is deposited alone.

At this point it was realized that the crystal monitor could not be relied upon to give accurate calibration data for the S deposition rates. A number of films were prepared using a constant (50 W) beam to sputter Mo and varied S sputter powers, and analyzed by RBS to determine their S/Mo ratios. The S deposition rates were then calculated using the equation

$$D_{\text{S}} = 1.647 D_{\text{Mo}} (S/\text{Mo}) \quad [3]$$

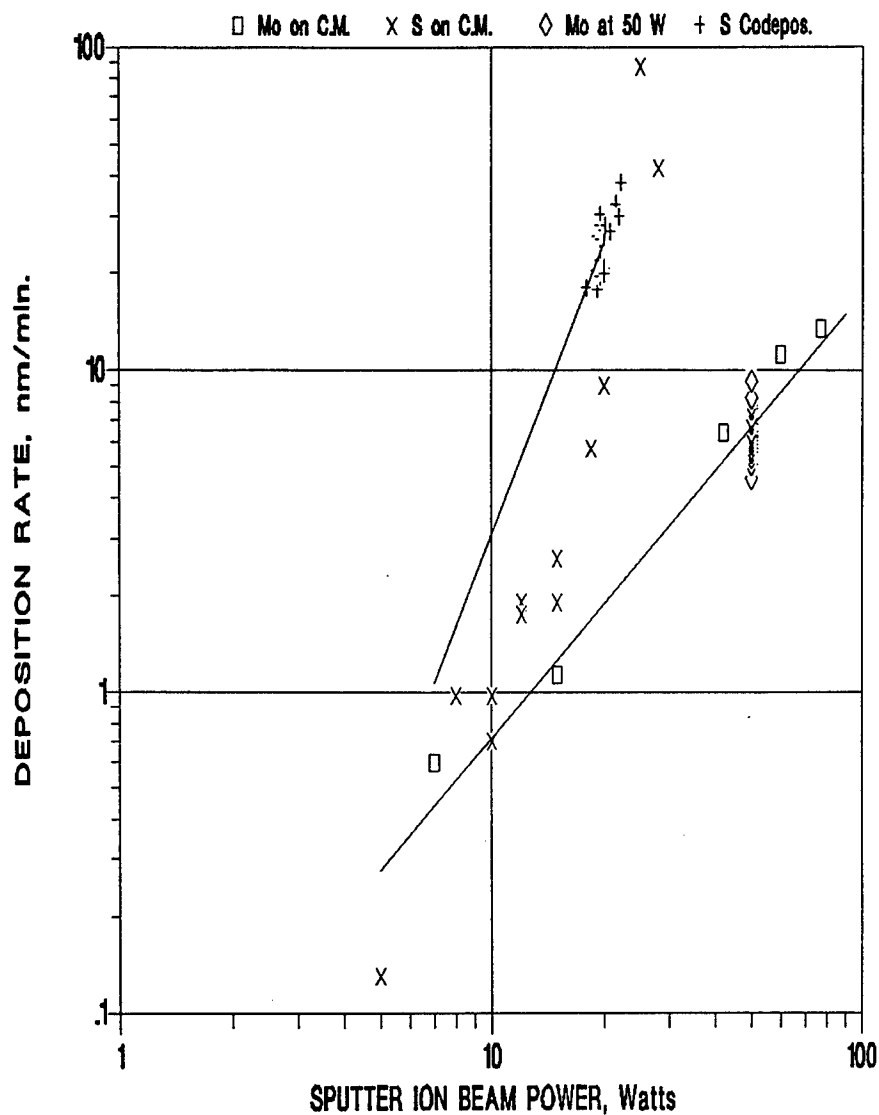


Fig. 7 - Deposition rates vs sputter powers for Mo and S on the crystal monitor, 19 points for Mo sputtered at 50 W, 18 points for S codeposited with Mo, and the regression lines of Eqs. [9] and [10].

based on the fact that the atomic density of Mo is 1.647 times that of S. The value of D_{Mo} was that from the Eq. [2] using 50 W as the power. From 13 data points a regression line having the equation

$$D_S = 0.00039 P_S^{3.7} \quad [4]$$

was found. The relatively high sputter rate for S is not unexpected, as sputter rates for various materials have been shown to increase rapidly when their temperatures were brought up to within about 200° of their melting points (10). Not only does S have a low melting point, but its relatively low thermal conductivity allows the target surface to be heated more by the ion beam. This causes accelerated sputtering and loss of control at higher beam powers.

Film deposition rates (D_F) can be calculated from the molecular weight and density of MoS_2 and the atomic weights and densities of Mo or S, as experiments have shown that IBAD MoS_2 is normally deposited with nearly bulk density (1). The film deposition rate is that of the MoS_2 , either

$$\frac{160.07 \times 10.2 \times D_{\text{Mo}}}{4.8 \times 95.94} = 3.545 D_{\text{Mo}}$$

or

$$\frac{160.1 \times 2.07 \times D_{\text{S}}}{4.8 \times 32.06 \times 2} = 1.077 D_{\text{S}}$$

plus that of the excess element from Eq. [3],

$$D_{\text{S}} - D_{\text{Mo}} \times 2 \times 1.647 = D_{\text{S}} - 3.294 D_{\text{Mo}}$$

or

$$D_{\text{Mo}} - \frac{D_{\text{S}}}{3.294} = D_{\text{Mo}} - 0.304 D_{\text{S}}$$

which can be simplified to give:

$$\text{For } S/Mo \geq 2: D_F = 0.251 D_{Mo} + D_S, \quad [5]$$

$$\text{For } S/Mo < 2: D_F = 0.773 D_S + D_{Mo}. \quad [6]$$

Improved Mo and S Data

After accumulating data for 27 films analyzed by RBS, more accurate constants for Eqs. [2] and [4] were obtained. For 19 films deposited using P_{Mo} of 50 W, the Mo deposition rates were determined from measured film deposition rates and the RBS S/Mo ratios (diamond markers in Fig. 7). The equations used were derived by combining Eq. [3] with Eq. [5] or [6]:

$$\text{For } S/Mo \geq 2: D_{Mo} = D_F / (0.251 + 1.647 (S/Mo)) \quad [7]$$

$$\text{For } S/Mo < 2: D_{Mo} = D_F / (1.273 (S/Mo) + 1) \quad [8]$$

The geometric mean of these rates was used to correct the coefficient of Eq. [2] to give

$$D_{Mo} = 0.030 P_{Mo}^{1.38} \quad [9].$$

Corrected S rates were then determined from 18 of the 27 films, excluding those with ion/atom (R) ratios > 0.08 and $S/Mo > 3$ or < 1.5 . The films with higher R's were excluded because the assist beam sputters the film, especially the S, reducing the growth rate. Eq. [3] was used again to find D_S , using the RBS S/Mo ratios and D_{Mo} 's calculated using Eq. [9]. The resulting replacement for Eq. [4] was

$$D_s = 0.0031 P_s^{3.0} \quad [10].$$

Although Eqs. [4] and [10] appear to have quite different slopes and intercepts, the lines intersect at 17 W and are quite close in the region where most of the films were made. For these 18 films, the mean of the measured D_F divided by that from Eq. [5] or [6] was 0.99 ± 0.19 and the mean of the RBS S/Mo divided by that from Eq. [3] solved for S/Mo was 1.02 ± 0.15 .

Shown in Fig. 7 are the adjusted regression line of Eq. [9] for Mo, the 18 points for S codeposited with Mo (+ markers), and the line for Eq. [10].

When the measured and calculated deposition rates for 122 films were compared, it was noted that a group of films having measured rates > 27 nm/min straggled away from the rest. These appeared to have high S/Mo ratios and low densities, and may have resulted from abnormally high S sputter rates.

Assist Beam Effects

When the ratio of measured / calculated rates were plotted as a function of R (assist beam ions / film atoms deposited), loss due to sputtering by the assist beam was readily apparent. This plot is shown in Fig. 8 with the high-rate data ($D_F > 27$ nm/min) shown but separated from the normal rate data ($D_F < 27$ nm/min). A suitable corrected calculated rate derived from the slope of the solid line was

$$D_F' = D_F(1 - 2.5R) \quad [11].$$

$$(R \leq 0.4)$$

The assist beam R was calculated from the molecular weight and density of MoS_2 , number of atoms per molecule, elementary

DEPOSITION RATE RATIO: MEASURED / CALCULATED

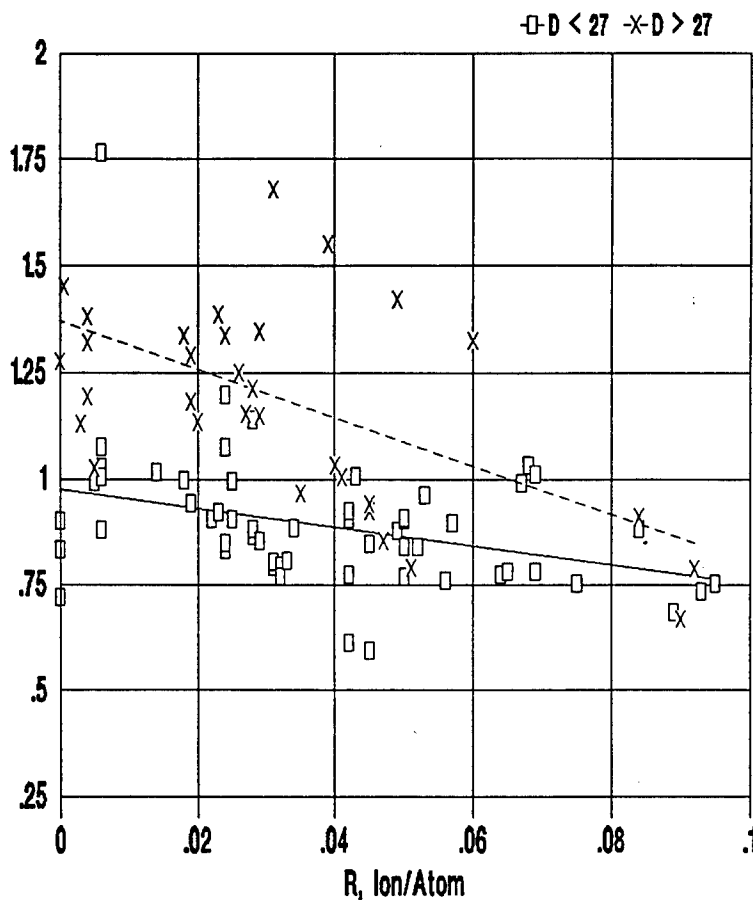


Fig. 8 - Ratio of measured to calculated film deposition rates vs assist beam ion per atom ratios for IBAD MoS_2 films deposited at normal ($D < 27$ nm/min.) and high ($D > 27$ nm/min.) rates.

charge, Avogadro constant, measured deposition rate, and beam flux. The latter was the experimentally determined Eq. [1] times a correction factor for decreasing beam flux with off-axis distance. For pure MoS_2 and a beam flux correction of 0.5 this calculation is:

$$\frac{(160 \text{ g} \cdot \text{Mole}^{-1} \times 6.25 \times 10^{12} \text{ Ion} \cdot \mu\text{A}^{-1} \cdot \text{s}^{-1} \times 3.8 \times I_B^{1.09} \mu\text{A} \cdot \text{cm}^{-2} \times 0.5 \times 60 \text{ s} \cdot \text{min}^{-1} \times 10^7 \text{ nm} \cdot \text{cm}^{-1})}{(4.8 \text{ g} \cdot \text{cm}^{-3} \times 3 \text{ Atom} \cdot \text{Molec.}^{-1} \times 6.02 \times 10^{23} \text{ Molec.} \cdot \text{Mole}^{-1} \times D_F \text{ nm} \cdot \text{min}^{-1})}$$

which reduces to

$$R = 0.13 I_B^{1.09} / D_F \quad [12]$$

in ions/atom where D_F was determined from the measured film thickness in nm and the duration of the deposition in minutes.

In order to have a means of calculating R from the sputter and assist ion source parameters and independent of the assumed stoichiometry and density of MoS_2 , the equation

$$R = 0.012 I_B^{1.09} / (0.106 D_{\text{Mo}} + 0.0646 D_S) \quad [13]$$

was derived in the same manner as Eqs. [5] and [6] and again includes the 0.5 correction factor. For all films the R's determined by both methods agreed within a factor of 2, and the agreement was much better when the high-rate films were excluded. The R's from Eq. [12] were about 1.25 x higher than those from Eq. [13] because the former were based on the final film thickness while the latter were based on the arrival of Mo and S at the substrate and did not allow for sputtering loss. Although the R from Eq. [12] has been used as a film parameter in our previous studies, that from Eq. [13] may be more fundamentally important, as it shows what mix of atoms and ions arrived at the substrate to interact and form the film. An iterative correction using Eq. [11] can be applied to Eq. [12] to give R as a ratio to the arriving atoms:

$$R' = R (1 - 2.5 R)$$

[14]

$$(R \leq 0.15).$$

The conformance is shown in Fig. 9, where the ratios based on film thickness and Eq. [12] as corrected by Eq. [14] can be compared with those based on the atom and ion arrival rates and Eq. [13]. Similarly, the inverse of Eq. [14] can be used to convert Eq. [13] to the ratio of ions per atoms in the finished film:

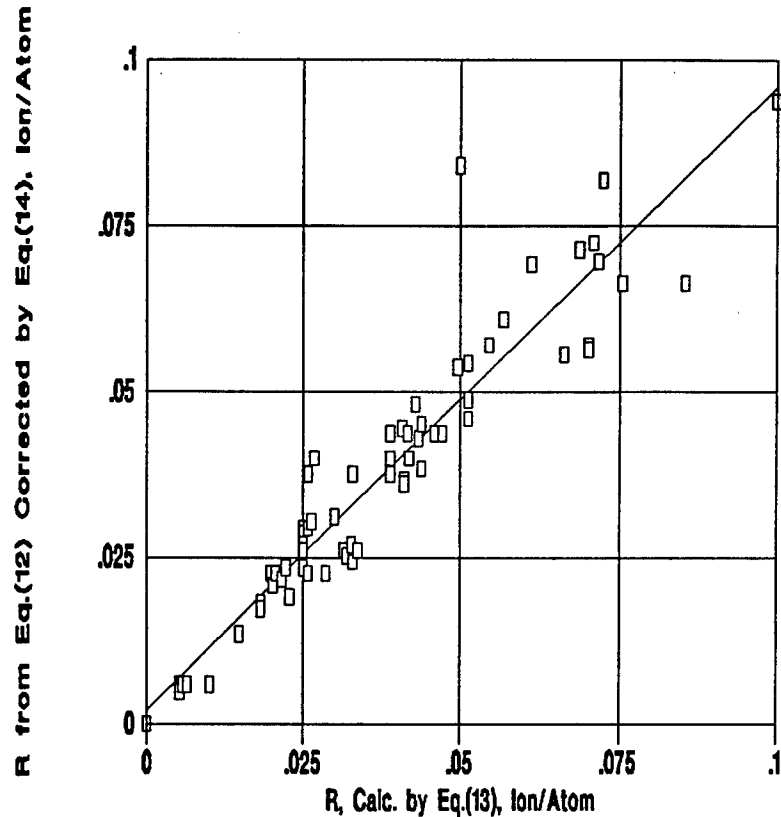


Fig. 9 - Conformance of ion/atom ratios based on the film thicknesses and corrected for sputtering losses with those calculated from atom and ion arrival rates.

$$R' = (1 - \sqrt{1 - 10 R}) / 5$$

[15]

$$(R \leq 0.09).$$

Film and Process Parameter Calculation Summary

In summary, to calculate the film parameters from the process parameters (beam powers) Eqs. [9] and [10] are used to find the

elemental deposition rates. Eq. [3] is rearranged and solved for the S/Mo ratio, and the appropriate Eq. [5] or [6] is used to find the film deposition rate. The arrival-based R is found from Eq. [13], and then the sputter loss correction of Eq. [11] can be applied to the rate. If R based on the finished film thickness is preferred, the correction of Eq. [15] can be applied.

To find the process parameters needed to produce a desired film, Eq. [9] is combined with Eq. [10] solved for P_s and Eq. [3] to give

$$P_s = 3.23 P_{Mo}^{0.46} \quad [16]$$

when S/Mo is taken as 2.1 to provide a slight excess of S. A Mo sputter power is then chosen in the range of 50 to 65 W. Lower powers allow better control, as the S deposition increases rapidly at higher powers. To set the assist beam current, an expected D_F is calculated from Eq. [9], [10], and [5]. Then from the same considerations as for Eq. [12],

$$I_B = (3.77 R D_F / 0.5)^{0.91} \quad [17]$$

where 0.5 is the off-axis beam flux correction and D_F is in nm/min. In practice, the constant was multiplied by 6 so that the rate was in Å/s (the units displayed by the crystal monitor) and multiplied by 1.6 to compensate for the "tooling factor" to give

$$I_B = (72 R D_F)^{0.91} \quad [18]$$

and a table for the desired R and a range of rates was prepared. During deposition the current was adjusted in accordance with the table for the rate measured by the crystal monitor.

Composite Mo-S Target

For coating non-planar substrates and forming films of MoS_2 alloyed with other metals a means of sputtering a controlled ratio of Mo and S from a single target was desired. Kuwano and Nagai (11) used a composite target to vary the stoichiometry in their deposition of MoS_2 and WS_2 films. A sulfur target was overlaid by overlapping fan-shaped segments of metal foil. The stoichiometry was changed by altering the angle of overlap. In their system, using a large target and relatively low beam intensity, areas of 68% S and 32% Mo were found to give films with $\text{S/Mo} = 2$. This arrangement provides little cooling for the Mo foil, which could get quite hot in our smaller but more intense beam. Aiming and stability of the beam would also be more critical, because movement of the beam off of the center of the sectors would change the sputtering ratio. With our apparatus, the high sputter yield of S relative to that of Mo and their different responses to beam power as shown by Fig. 7 and Eqs. [9] and [10] indicated that a composite target with a relatively low S area would be needed to give films with a S/Mo ratio of 2, and that the ratio could be adjusted by changing the sputter beam power.

An experimental composite target was prepared by drilling shallow holes in a Mo target as shown in Fig. 10. Twelve holes of 0.20 inch (5.1 mm) diameter were made in a square grid pattern with a 5/8 inch (1.6 cm) spacing, and then filled with molten sulfur by placing powdered S in them and heating the target. After the target cooled and the S solidified, the surface was scraped and abraded to remove any excess S. The resulting S and Mo areas in the central portion of the target were 8% S and 92% Mo. Gradual cooling of the molten S was found to be important to prevent cracking. Cracks interfere with heat transfer through the S to the Mo, causing melting and rapid loss of the S.

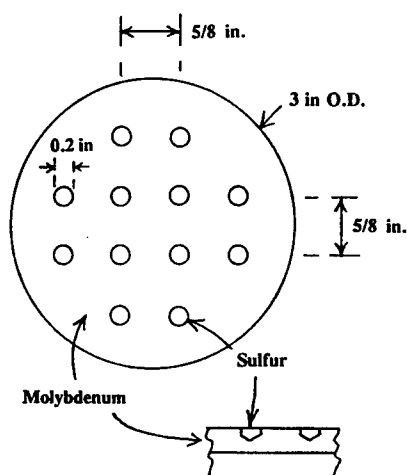


Fig. 10 - Composite molybdenum and sulfur sputtering target.

This target performed reasonably well for thin films, though the deposition rate had to be held down to avoid high S/Mo ratios (12). The target required replenishment after each use to maintain the S yield, and also tended to produce excessive amounts of S at the start of a deposition, then decreasing amounts as the reservoirs were depleted. Figure 11, for example, shows the composition with depth from RBS data of an MoS_x + Pb film prepared by sputtering at constant powers from a Pb target and the composite Mo + S target. The initial deposit was too rich in S, with $\text{S/Mo} > 8$, while the final deposit at the surface was about that desired, $\text{S/Mo} \approx 2$. The best endurance was obtained with minimal excess S.

Deposition of Various Metals

In order to make metal-alloyed MoS_2 films and mixed metal films, several metals have been deposited at different beam powers to determine their rates for 11.9 cm target to substrate distances. All of these yielded rate vs beam power plots with slopes similar to that of Mo data shown in Fig. 7. There was no systematic variation in these slopes, and their differences were not great compared with their statistical uncertainties. It was therefore considered likely that a formula

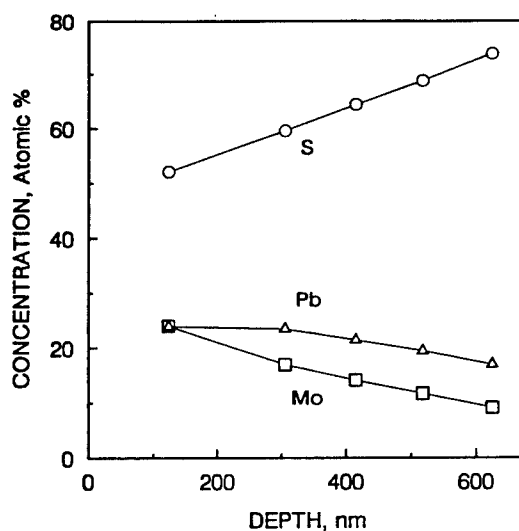


Fig. 11 - Composition vs depth profile of a film deposited by sputtering from Pb and composite Mo + S targets.

with a fixed exponent and different coefficients would adequately fit the data. A weighted mean of the exponents gave 1.45, so the data for each metal were fitted to:

$$D_{\text{■}} = C P_{\text{■}}^{1.45} \quad [19].$$

The coefficients, C, for the metals were: W: 0.011, Mo: 0.0236, Ni: 0.031, Co: 0.034, Cu: 0.045, and Pb: 0.11. Between 25 and 50 watts, the rates calculated with this equation and those using individual exponents did not differ by more than 10%. The Mo rate did not vary more than 3% from that calculated with Eq. [9]. Most discrepant were the results for Pb.

Effect of Target Distance

Although the sputtered areas on the targets are not point sources, it was found in this work that the difference in deposition rate at a given power could be adequately estimated from the inverse of the squares of the radii:

$$D_1 / D_2 = r_2^2 / r_1^2 \quad [20]$$

where r is the radius (distance from the target to the substrate). This makes possible the modelling of dual target deposition from geometric considerations and individual deposition rates, and was used to correct some of the data for metals which were sputtered from radii other than 11.9 cm.

Uniformity of Deposition

Since the distances from the targets to various points on the platen differ substantially, the instantaneous deposition rates across it are not uniform. Rotation of the platen reduces this problem but cannot eliminate it since the gradient is not linear. Experiments have shown that substrates at the platen edge receive

about 80% as much thickness as at the center.

Intentional Composition Gradients

Films with compositions varying across the surface can be made by cosputtering from two different targets onto a non-rotating substrate. Mixed metal films on glass for a study of double-oxide friction were prepared in this manner. A metal plate long enough to support two microscope slides end-to-end was fastened to the platen, and the stage was moved to its lowest position and centered. The plane of the substrates was 16 cm below the target centers, which were 9.5 cm from the chamber center plane. The slides were positioned with their lengths perpendicular to the center plane and extending 7.6 cm from it. For any position P along the substrate a distance LP from the left end, the radii from the left (L) and right (R) targets were

$$r_L^2 = 260 + 3.8 LP + LP^2 \quad [21]$$

$$r_R^2 = 549 - 34 LP + LP^2 \quad [22].$$

Expected deposition rates at points along the substrates could be predicted from Eq. [19] corrected by Eq. [20] for the radii found from Eq. [21] and [22]. The expected totals could be compared with rates from measured thicknesses, and the theoretical rate and composition profiles adjusted to fit. With the beam powers set to give equal rates from both targets, the composition was predicted to be 67% of metal from the closer target at each end with a reasonably linear gradient to equality in the center.

SUMMARY

The apparatus and techniques used for ion-beam-assisted deposition of films, principally of MoS₂ on top of a base layer of TiN, are described. The most efficient technique for depositing the

MoS₂ was found to be by codeposition of Mo and S from separate targets. The Mo and S deposition rates and assist ion flux have been measured and simple formulae have been found to relate them to the operating parameters. This allows films of the desired MoS₂ composition and optimum assist ratio to be prepared using parameters calculated by Eqs. [16] and [18]. Alloyed and graded-composition metal films can likewise be prepared using the guidance of Eqs. [19] through [22].

ACKNOWLEDGMENTS

We would like to thank the S.D.I. Organization for equipment funding, SDIO and NRL/ONR for program funding, Graham Hubler of NRL for advice on Faraday cup design and the effect of ion source operating parameters on the beam properties, and C.R. Gossett, SFA, Inc., for Rutherford backscattering analyses.

REFERENCES

1. Bolster, R.N., Singer, I.L., Wegand, J.C., Fayeulle, S., and Gossett, C.R., "Preparation by Ion-Beam-Assisted Deposition, Analysis, and Tribological Behavior of MoS₂ Films," *Surf. Coat. Technol.*, 46, pp. 207-216 (1991).
2. Seitzman, L.E., Singer, I.L., Bolster, R.N., and Gossett, C.R., "Effect of a Titanium Nitride Interlayer on the Endurance and Composition of a Molybdenum Disulfide Coating Prepared by Ion-Beam-Assisted Deposition," *Surf. Coat. Technol.* 51, pp. 232-236 (1992).
3. Seitzman, L.E., Bolster, R.N., and Singer, I.L., "X-Ray Diffraction of MoS₂ Coatings Prepared by Ion-Beam-Assisted Deposition," *Surf. Coat. Technol.* 52, pp. 93-98 (1992).

4. Kaufman, H.R., "Technology and Applications of Broad-Beam Ion Sources Used in Sputtering. Part I. Ion Source Technology," *J. Vac. Sci. Technol.*, 21, pp.725-736 (1982).
5. Harper, J.M.E., Cuomo, J.J., and Kaufman, H.R., "Technology and Applications of Broad-Beam Ion Sources Used in Sputtering. Part II. Applications," *J. Vac. Sci. Technol.*, 21, pp.737-756 (1982).
6. Kuwano, H., and Nagai, K., "Friction-Reducing Coatings by Dual Fast Atom Beam Technique," *J. Vac. Sci. Technol.*, A 4, pp. 2993-2996 (1986).
7. Harper, J.M.E., Cuomo, J.J., and Hentzell, H.T.G., "Quantitative Ion Beam Process for the Deposition of Compound Thin Films," *Appl. Phys. Lett.*, 43, pp. 547-549 (1983).
8. Rossnagel, S.M., and Cuomo, J.J., "Film Modification by Low Energy Ion Bombardment During Deposition," *Thin Solid Films*, 171, pp. 143-156 (1989).
9. Hubler, G.K., "Fundamentals of Ion-Beam Assisted Deposition: Technique and Film Properties," *Mater. Sci. Eng. A, Struct. Mater., Prop. Microstruct. Process. (Switzerland)*, A115, pp. 181-192 (1989).
10. Kelly, R., "Thermal Effects in Sputtering," *Surface Sci.*, 90, p. 280 (1979).
11. Kuwano, H., and Nagai, K., "Thin Solid Lubricant Film Formation by Fast Atom Bombardment Sputter Deposition," *J. Vac. Sci. Technol.*, A 3, pp. 1809-1812 (1985).
12. Bolster, R.N., and Singer, I.L., "IBAD MoS₂ Film Deposition From a Composite Target," NRL Letter Report 6170-431A of 17 October 1990